Elastic behavior, phase transition, and pressure induced structural evolution of analcime

G. Diego Gatta,[1,2,*] Fabrizio Nestola,[2,3] and Tiziana Boffa Ballaran[2]

[1]Dipartimento di Scienze della Terra, Universita' degli Studi di Milano, Via Botticelli 23, I-20133 Milano, Italy
[2]Bayerisches Geoinstitut, Universitaet Bayreuth, Universitaetsstrasse 30, D-95447 Bayreuth, Germany
[3]Crystallography Laboratory, Department of Geosciences, Virginia Tech, Blacksburg, Virginia 24061, U.S.A.

Abstract

Elastic and structural behavior of a natural cubic analcime (space group: $Ia\overline{3}d$) from Sardinia (Italy) was investigated at high pressure by in situ single-crystal X-ray diffraction. A first-order phase transition is observed in the pressure range between 0.91(5) and 1.08(5) GPa. Unit-cell constants and reflection conditions confirm that the space group of the HP-polymorph is $P\overline{1}$. No further phase-transition has been observed at least up to 7.14 GPa. Fitting the volume data of the cubic polymorph with a second-order BM-EoS we obtain: $V_0 = 2571.2(4)$ Å^3, $K_{T0} = 56(3)$ GPa, and $K' = 4$ (fixed). For the triclinic polymorph, a third-order EoS gives: $V_0 = 2607(9)$ Å^3, $K_{T0} = 19(2)$ GPa, and $K' = 6.8(7)$. Axial bulk moduli of the triclinic polymorph, calculated with a linearized BM-EoS, are: $K_{T0}(a) = 29(2)$ GPa, with $K'(a) = 4.9(6)$ and $a_0 = 13.727(10)$ Å; $K_{T0}(b) = 20(1)$ GPa, with $K'(b) = 5.2(5)$, and $b_0 = 13.751(15)$ Å; $K_{T0}(c) = 11(1)$ GPa, with $K'(c) = 12.6(6)$ and $c_0 = 13.822(31)$ Å. The elastic behavior of the HP-polymorph appears to be strongly anisotropic, being $K_{T0}(a):K_{T0}(b):K_{T0}(c) = 2.64:1.82:1.00$. The relevant structural variations in response to the cubic $\rightarrow$ triclinic phase transition are due to tetrahedral tilting. The tetrahedral framework distortion gives rise to a change of the eight- and six-ring channels ellipticity and of the extra-framework topological configuration: it appears in fact that for the high-pressure triclinic polymorph the coordination number of some of the Na atoms is seven ($2H_2O$ + five framework O atoms) instead of six ($2H_2O$ + four framework O atoms).

Key words: Analcime, zeolite, high-pressure, compressibility, phase transition

Introduction

Analcime (or analcite) is commonly defined as feldspathoid, with ideal formula $NaAlSi_2O_6 \cdot H_2O$, although the Commission of the International Mineralogical Association included analcime in the zeolite group (Coombs et al. 1997). Analcime occurs in a wide variety of geological environments and for several decades has been the object of a debate concerning its genetic conditions and origin (primary or secondary). Natural occurrences and experimental evidences appear to confirm that both primary and secondary analcime exist (Roux and Hamilton 1976; Woolley and Symes 1976; Wilkinson 1977; Luhr and Kyser 1989; Gianpaolo et al. 1997; Redkin and Hemley 2000; Prelević et al. 2004). However, whereas primary analcime has rarely been found (in rocks like blairmorites or minettes, Woolley and Symes 1976; Wilkinson 1977; Luhr and Kyser 1989), many secondary analcimes has been observed as the products of alteration of primary magmatic minerals, like nepheline and leucite (Gianpaolo et al. 1997; Redkin and Hemley 2000; Prelević et al. 2004 and references therein).

The crystal structure of analcime was first solved by Taylor (1930) by means of single-crystal X-ray diffraction in the space group $Ia\overline{3}d$. Cubic symmetry was confirmed by Ferraris et al. (1972) and Line et al. (1996) by means of single-crystal and powder diffraction respectively using a neutron source, giving new insight into the topological configuration of the water molecules into the structural channels. Several studies have shown that analcime can deviate from cubic symmetry (Coombs 1955; Mazzi and Galli 1978; Hazen and Finger 1979; Pechar 1988; Kapusta and Wlodyka 1997; Takaishi 1998; Yokomori and Idaka 1998). Mazzi and Galli (1978) reported for natural analcimes deviation from cubic to tetragonal and to orthorhombic symmetry on the basis of single-crystal X-ray diffraction data. The authors proposed a model to explain the deviation from the cubic symmetry: the crystal structure of pseudo-cubic analcime is considered to be made up of one "basic tetragonal structure" (with $a > c$), which is statistically oriented in three mutually orthogonal directions (around the [111] of the cubic lattice). Small domains of the basic "tetragonal $a > c$" structure, differently oriented, would explain the pseudo-cubic cell constants and the lower symmetry. Hazen and Finger (1979) reported a comparative study of 19 natural samples of analcime, based on lattice constants (measured by single-crystal X-ray diffraction), chemical analysis, and optical parameters. The authors distinguished between cubic, tetragonal, orthorhombic, monoclinic, and triclinic symmetry on the basis of the lattice parameters. Pechar (1988) reported the crystal structure of a natural monoclinic analcime obtained by means of single crystal X-ray and neutron diffraction. Takaishi (1998) and Yokomori and Idaka (1998) reported evidence that the ideal topological symmetry can be described by a trigonal lattice. The reason for such a wide range of symmetries is still unclear although, as stated by several authors (Mazzi and Galli 1978; Hazen and Finger 1979), different Si/Al-distributions might be one of the explanations. Moreover, it is still not known how the

* E-mail: diego.gatta@unimi.it

genetic conditions (*P*, *T*, *X*) control the different stability fields of analcime.

The crystal structure of analcime is built up of the combination of two "secondary buildings units" (SBU): 4 and 6 SBU (four and six-membered rings of tetrahedra, Baerlocher et al. 2001) and belongs to the "ANA group" (with analcime and isotypic minerals such as leucite, wairakite, pollucite, hsianghualite; Armbruster and Gunter 2001; Baerlocher et al. 2001). Gottardi and Galli (1985) first defined the analcime group as "zeolites group with singly connected four-ring chains". The framework topology of the ANA group shows the maximum symmetry ($Ia\bar{3}d$, Baerlocher et al. 2001). In cubic analcime there is a statistical Si/Al-distribution in the tetrahedral framework and the Na sites are statistically two thirds occupied (due to charge balance). The Na sites are six-coordinated (with four O atoms belonging to the tetrahedral framework and two to the water molecules) and extend into the framework voids. Two different systems of channels can be observed in the crystal structure of analcime: irregular channels formed by highly distorted eight-membered rings (8mR), and regular channels formed by six-membered rings (6mR) along the [111] direction of the cubic lattice. The lower symmetry structures show some Si/Al-ordering (Mazzi and Galli 1978; Pechar 1988). Similar evidence for non-cubic analcimes has also provided by ^{29}Si MAS NMR studies (Kato and Hattori 1998; Cheng et al. 2000; Neuhoff et al. 2003 and references therein).

A limited number of studies have been devoted to analcime under non-ambient conditions. Calorimetric and phase equilibrium studies of the low- and high-temperature (HT) behavior of analcime were investigated by Liou (1971), Kim and Burley (1971, 1980), Gottardi and Galli (1985), Putnis et al. (1993), Line (1995), Line et al. (1995), and Cruciani and Gualtieri (1999). The HT-structural evolution of a tetragonal analcime was studied by Cruciani and Gualtieri (1999) by means of in situ synchrotron powder diffraction up to 1064 K. At 650 K they observed a complete loss of water and some evidence of evolution toward cubic structure at HT. A low-temperature (LT) study of cubic analcime down to 30 K showed that no phase transition occurs within the *T*-range investigated (Line et al. 1996). Yoder and Weir (1960) reported that analcime undergoes a reversible phase transition at about 0.8 GPa on the basis of high pressure (HP) X-ray powder diffraction. Hazen and Finger (1979) studied the high-pressure (HP) behavior of two natural analcimes (tetragonal and orthorhombic) up to 2.5–3.0 GPa by means of single-crystal X-ray diffraction. Based on unit-cell discontinuities observed for both crystals, the authors suggested that two phase transitions occur, the first to monoclinic and the second to triclinic symmetry. No structural refinement was performed. Goryainov et al. (1996) and Miroshnichenko and Goryainov (2000) studied the HP-behavior of fully hydrated and dehydrated analcimes up to 2.5 GPa by means of Raman spectroscopy and optical microscopy. The authors observed two discontinuities in the HP Raman spectra that they considered to be phase transitions (at ~0.8 and ~2.0 GPa for hydrated analcime and at ~0.37 and ~1.1 GPa for dehydrated analcime), suggesting that the transition pressures are higher in hydrated crystals.

The aim of our study is to investigate the elastic behavior and the HP-structural evolution of cubic analcime under hydrostatic regime by in situ single-crystal X-ray diffraction. Current HP-facilities and improvements in diffractometers and detectors can now provide us with more accurate and precise data up to pressure values higher than those reached in the previous studies, allowing us to investigate the crystal structure of the HP-polymorphs, which is still unknown. A comparison between the HP and LT-HT behavior of analcime was also be carried out.

EXPERIMENTAL METHODS

The analcime specimen investigated in this study comes from Su Marralzu, Sardinia, Italy, (n. 35 of the zeolite collection of the Dipartimento di Scienze della Terra, Università di Perugia, Italy) and was kindly provided by Prof. R. Rinaldi. Part of a natural, colorless, transparent, and gem-quality single crystal of analcite (~1.5 cm^3) was cut into three parts to perform the optical observations, chemical analysis, and HP single-crystal diffraction experiments.

In transmitting polarized light the crystal prepared as a thin section (thickness: 30 μm) appeared free of defects, homogeneous, and absolutely isotropic. As stated by Mazzi and Galli (1978), non-cubic crystals of analcime are always polysynthetically twinned and show a weak, but appreciable, birefringence.

Electron microprobe analysis in WDS was performed using a fully automated CAMECA SX-50 microprobe. Major and minor elements were determined at 15 kV accelerating voltage and 10 nA beam current with a counting time of 20 seconds. To minimize loss of water due to the electron bombardment, the crystal was mounted in epoxy resin and a defocused beam was used, following the same protocol adopted by Gatta and Boffa Ballaran (2004). The standards employed were: albite (Al, Si, Na), microcline (K), and anorthite (Ca). The chemical content (obtained by averaging 15 point analyses) is Na$_2$O 12.620%, K$_2$O 0.015%, CaO 0.017%, Al$_2$O$_3$ 21.170%, SiO$_2$ 57.960%, and H$_2$O 8.217% (by difference) with a resulting chemical formula, calculated on the basis of seven oxygen atoms, of (Na$_{0.887}$K$_{0.001}$Ca$_{0.001}$)(Al$_{0.905}$Si$_{2.102}$)O$_6$·0.994H$_2$O.

A single crystal (180 × 160 × 60 μm^3) was used for the diffraction experiments. Accurate unit-cell constants were measured with the crystal in air (Table 1) with a Huber four-circle diffractometer (non-monochromatized Mo$K\alpha$ radiation) using eight-position centering of 24 Bragg reflections according to the procedure of King and Finger (1979) and Angel et al. (2000) (Table 1). The centering procedure and vector-least-square refinement of the unit-cell constants were performed using the SINGLE04 software according to the protocol of Ralph and Finger (1982) and Angel et al. (2000). The unrestrained cell constants showed an isometric lattice (deviations from the constrained values were less than 2σ). Diffraction data were then collected with an Xcalibur-Oxford Diffraction diffractometer (Kappa geometry, graphite-monochromated Mo$K\alpha$ radiation). Details of the data collection procedure are reported in Table 2. No restraint, in terms of the reflections conditions, was applied during the data collection. The reflection conditions observed are in agreement with a $Ia\bar{3}d$ space group. Only one violation was found, represented by the (002) reflection, which may suggest an orthorhombic space group (*Ibca* according to Mazzi and Galli 1978). However, its intensity was only $I \sim 5\sigma(I)$. An empirical absorption correction was performed using the CrysAlis1.170 software package provided by Oxford Diffraction (2003). Intensity data were corrected for Lorentz-polarization effects. The crystal structure refinement was performed with anisotropic displacement parameters in space group $Ia\bar{3}d$ using the SHELX-97 software (Sheldrick 1997), starting from the atomic coordinates of Line et al. (1996). The hydrogen atoms were not considered, since they could not be detected during the HP-experiments. Neutral atomic scattering factors of Na, Si, and O were used according to the International Tables for Crystallography (Wilson and Prince 1999). No peak larger than ±0.35 e^-/Å^3 was present in the final difference-Fourier synthesis at the end of the refinement. Details of the structural refinement are reported in Tables 2 and 3. The tetrahedral bond distances are indicative of Si/Al-disordering (Table 3). A further refinement performed in the *Ibca* space group was unsuccessful with an agreement index [$R_1(F)$] 2.5 times larger than that obtained using the cubic structure. We can therefore infer that our analcime sample is cubic.

A BGI diamond-anvil cell (Allan et al. 1996) was used for the HP-experiment. Steel T301 foil, 250 μm thick, was used as gasket. The gasket foil was pre-indented to a thickness of about 110 μm before drilling a hole (~350 μm) by spark-erosion. The same platy crystal of analcime previously studied at ambient conditions was placed into the gasket hole together with some ruby chips, used for pressure calibration according to Mao et al. (1986), with uncertainties in the measured pressure of about ~0.05 GPa. A methanol:ethanol:water (16:3:1) mixture was used as a hydrostatic pressure-transmitting medium (Miletich et al. 2000). Accurate lattice parameters were determined at ambient temperature and at pressures ranging be-

TABLE 1. Lattice parameters of analcime at different pressures

P (GPa)	a (Å)	b (Å)	c (Å)	α (°)	β (°)	γ (°)	V (Å³)
0.0001	13.7065(8)						2575.0(5)
0.0001*	13.6999(3)	–	–	–	–	–	2571.3(4)
0.10(5)	13.6917(4)	–	–	–	–	–	2566.7(5)
0.30(5)	13.6746(4)	–	–	–	–	–	2557.1(5)
0.53(5)	13.6573(4)	–	–	–	–	–	2547.4(5)
0.80(5)	13.6373(2)	–	–	–	–	–	2536.2(3)
0.91(5)	13.6288(5)	–	–	–	–	–	2531.5(6)
1.08(5)	13.5707(7)	13.5345(12)	13.5277(12)	89.688(4)	89.251(4)	90.707(3)	2484.2(3)
1.23(5)	13.5574(3)	13.5119(4)	13.5082(5)	89.600(5)	89.162(3)	90.798(4)	2474.0(1)
1.30(5)	13.5388(4)	13.4912(9)	13.4859(6)	89.532(5)	89.084(3)	90.822(5)	2462.6(2)
1.50(5)	13.5080(5)	13.4573(14)	13.4485(7)	89.507(7)	88.821(4)	90.733(4)	2443.9(3)
1.71(5)	13.4872(4)	13.4240(16)	13.4142(7)	89.546(7)	88.545(4)	90.459(6)	2427.7(3)
1.82(5)	13.4734(3)	13.4036(3)	13.3880(4)	89.587(4)	88.376(2)	90.298(4)	2416.7(1)
2.06(5)	13.4551(4)	13.3728(13)	13.3561(4)	89.630(5)	88.212(2)	90.108(5)	2402.0(3)
2.12(5)	13.4464(4)	13.3657(5)	13.3449(7)	89.691(5)	88.152(3)	90.034(4)	2397.1(2)
2.48(5)	13.4074(4)	13.3069(11)	13.2866(5)	89.768(6)	87.881(3)	89.777(5)	2368.8(2)
2.99(5)	13.3608(7)	13.2496(17)	13.2269(7)	89.863(10)	87.631(5)	89.511(10)	2339.4(4)
3.35(5)	13.3221(5)	13.2006(13)	13.1829(5)	89.946(6)	87.452(3)	89.334(7)	2315.9(3)
3.84(5)	13.2717(7)	13.1449(13)	13.1330(6)	90.034(7)	87.247(4)	89.105(7)	2288.2(3)
4.34(5)	13.2225(6)	13.0876(11)	13.0877(6)	90.108(7)	87.065(4)	88.890(8)	2261.4(3)
5.04(5)	13.1605(7)	13.0149(18)	13.0335(8)	90.178(9)	86.849(4)	88.601(9)	2228.4(4)
6.23(5)	13.0660(5)	12.8985(13)	12.9511(7)	90.352(8)	86.528(4)	88.150(7)	2177.5(3)
7.14(5)	13.0123(4)	12.8276(10)	12.8730(4)	90.567(4)	86.281(2)	87.630(5)	2142.2(2)
0.0001†	13.7034(8)	–	–	–	–	–	2573.3(4)

* Data collected with the crystal in the DAC without *P*-medium.
† Data collected with the crystal in air after decompression.

TABLE 2. Details of data collection and refinements of analcime at different pressures

Pressure (GPa)	0.0001	0.0001*	0.91(5)	1.23(5)	2.12(5)	5.04(5)
Crystal size (μm)	180×160×60	180×160×60	180×160×60	180×160×60	180×160×60	180×160×60
Radiation	Mo*K*α	Mo*K*	Mo*K*α	Mo*K*α	Mo*K*	Mo*K*α
Unit-cell constants:						
a (Å)	13.7237 (5)	13.7101(7)	13.6372 (6)	13.5424 (4)	13.4353(1)	13.1413(2)
b (Å)				13.5010(40)	13.3611(20)	13.0080(16)
c (Å)				13.5038(3)	13.3399(1)	13.0222(2)
α (°)				89.543(7)	89.730(3)	90.077(3)
β (°)				89.182(2)	88.124(1)	86.847(1)
γ (°)				90.748(9	89.961(3)	88.668(4)
2θ range (°)	2-60	2-60	2-60	2-60	2-60	2-60
Scan type	ω	ω	ω	ω	ω	ω
Scan speed (°/s)	0.05	0.05	0.05	0.05	0.05	0.05
Scan width (°)	1.20	1.20	1.20	1.20	1.20	1.20
Detector-sample distance (mm)	135.0	135.0	135.0	135.0	135.0	135.0
Space group	*Ia*3̄*d*	*Ia*3̄*d*	*Ia*3̄*d*	*P*1̄	*P*1̄	*P*1̄
Reflections measured	2626	424	401	1203	1086	3628
Unique refl. (total)	307	144	147	913	992	1261
Unique refl. with $F_o > 4\sigma(F_o)$	263	81	78	702	605	779
Parameters refined	24	10	10	278	278	278
$R_{int}/R_{Friedel}$	0.069	0.069	0.097	0.086	0.012	0.069
R_1 (F)	0.021	0.077	0.096	0.171	0.184	0.187
GooF	0.928	1.148	0.961	1.190	1.100	0.839

Note: $R_{int} = \Sigma|F_{obs}^2 - F_{obs}^2(mean)|/\Sigma[F_{obs}^2]$ is calculated only on the basis of Friedel pairs for the three HP-triclinic structures; $R_1 = \Sigma(|F_{obs}| - |F_{calc}|)/\Sigma|F_{obs}|$.
* Data collected with the crystal in the DAC without *P*-medium.

tween 0.0001 and 7.14(5) GPa (Table 1) using 18 Bragg reflections and the same centering procedure used for the crystal in air.

Five data collections at 0.0001 GPa (with the crystal in the DAC without any pressure medium), 0.91(5), 1.23(5), 2.12(5), and 5.04(5) GPa (Table 2) were performed using the same procedure described for the crystal in air. Integrated intensity data were corrected for LP and absorption effects due to the crystal and pressure-cell using the ABSORB5.2 computer program (Burnham 1966; Angel 2002, 2003a,b). The Na occupancy was fixed to the value obtained for the crystal in air and was not refined. Isotropic displacement parameters were used. Refined atomic positions, thermal displacement parameters, and bond distances of cubic analcime are summarized in Table 3. For the triclinic HP-polymorph, the starting coordinates were generated from the cubic structure and then refined. The crystal structure of the triclinic polymorph was refined in the $P\bar{1}$ space group given the presence of a relevant number of $(h + k + l) \neq 2n$ reflections violating the body-centered lattice. Geometrical soft-restraints on the T-O and O-O bond distances of the tetrahedra were applied: the distances between T-O were restrained to a target

value of 1.650 Å with an estimated standard deviation of ± 0.015 Å and the O-O distances were restrained to 2.660 ± 0.020 Å. Isotropic displacement parameters were refined by grouping all of the Si, O, and Na atoms in three distinct groups (Table 4). Due to the large number of structural parameters, framework and extra-framework atoms were refined separately in a first set of cycles of refinements. After that, both were refined together although the ratio observations/parameters ≤3 was clearly non-ideal. These last cycles of refinements gave the same atomic positions, bond distances and angles within the e.s.d. previously obtained. More-over, (1) the variance-covariance matrix of the final refinements showed that no significant correlation between refined parameters occurred and (2) convergence was rapidly achieved and at the end of the refinements the shifts in all parameters were less than their e.s.d. values. The stability of the HP-refinements was basically improved by the geometrical soft restrains adopted, which act as if they were some additional experimental observations (Sheldrick 1997). Refined atomic positions and displacement parameters of the triclinic analcime at different pressures are reported in Table 4. Bond distances for framework and extra-framework polyhedra

TABLE 3. Refined atomic positions, site occupancy, thermal displacement parameters (Å^2), and bond distances for low-P cubic analcime

Site (Wyckoff pos.)	x	y	z	Site occupancy	U_{iso}/U_{eq}	Bond distances (Å)	
Na (24c)	0.125	0	0.25	0.570(6)	0.036(1)	Na-W (×2)	2.4260
	0.125	0	0.25	0.570	0.0374(6)		2.4236
	0.125	0	0.25	0.570	0.0351(7)		2.4107
Si/Al (48g)	−0.125	0.16224(3)	−0.08776(3)	1.00	0.0119(2)		
	−0.125	0.1616(3)	−0.0884(3)	1.00	0.012(1)	Na-O (×4)	2.507(1)
	−0.125	0.1617(3)	−0.0882(3)	1.00	0.012(1)		2.487(8)
O (96h)	−0.1160(1)	0.14526(9)	0.03049(8)	1.00	0.0332(5)		2.468(11)
	−0.1148(7)	0.1459(6)	0.0306(6)	1.00	0.025(3)		
	−0.1149(7)	0.1461(8)	0.0314(6)	1.00	0.035(3)	Si-O (×4)	1.644(1)
W (16b)	0.125	0.125	0.125	1.08(1)	0.092(3)		1.646(9)
	0.125	0.125	0.125	1.08	0.091(10)		1.631(9)
	0.125	0.125	0.125	1.08	0.098(13)		

Note: For each site, the values from top to bottom correspond to the refinement at 0.0001 GPa (in air), 0.0001 GPa (with crystal in the DAC), and 0.91(5) GPa. For the refinement at 0.0001 (with the crystal in the DAC) and at 0.91(5) GPa the isotropic thermal parameters, U_{iso}, are reported, whereas for the refinement with the crystal in air U_{eq} are shown.

are reported in Tables 5 and 6, respectively, which are deposited.[1] Observed and calculated structure factors are deposited (Table 7)[1] and can be obtained from the authors upon request.

RESULTS

Elastic behavior

The evolution of the unit-cell constants with pressure is shown in Figure 1. The isometric lattice is maintained at least up to 0.91(5) GPa. A first-order phase transition is observed in the pressure range between 0.91(5) and 1.08(5) GPa. The transition pressure was bracketed by several measurements in compression and decompression. The HP-polymorph shows a metrically triclinic lattice, for which the pseudo-tetragonal Mazzi's set (Mazzi and Galli 1978) with $a > b > c$ was adopted. The cubic $\rightarrow$ triclinic phase transition is reversible and without any appreciable hysteresis effect. Optical and diffraction observations did not show any phase transition-induced twinning of the crystal. In the P-range between 0.53(5) and 0.91(5) GPa the FWHMs of all Bragg reflections measured increased by about 30%. However, at $P \geq 1.08(5)$ GPa such effect disappears and the FWHM values become similar to those of the low-P polymorph. The evolution of the unit-cell constants with P appears continuous up to 7.14(5) GPa, with **a** being less compressible than the other two parameters, whereas an unusual HP-trend is observed for the α, β, and γ angles (Fig. 1). The α angle decreases up to 1.30-1.50 GPa and then increases with P, the β angle decreases within the P range investigated but a change in slope is observed at 1.30 GPa, γ first increases up to 1.30 GPa and then decreases. At 2.48 GPa, the α and γ values are very close (Fig. 1, Table 1).

The P-V data of the low-P polymorph were fitted with a second-order Birch-Murnaghan Equation-of-State (BM-EoS) (Birch 1947), with the EOS-FIT5.2 computer program compiled by Angel (2001). The elastic parameters obtained, using the data weighted by the uncertainties in P-V, are as follows: V_0

= 2571.2(4) Å^3, K_{T0} = 56(3) GPa, K' = 4 (fixed). A third-order BM-EoS was instead used for the HP-polymorph, yielding the following values: V_0 = 2607(9) Å^3, K_{T0} = 19(2) GPa, K' = 6.8(7). The axial compressibility coefficients were calculated in terms of "axial bulk moduli" with a "linearized" BM-EoS (Angel 2000), substituting the cube of the lattice parameter for the volume. The elastic parameters for the HP-polymorph obtained using a third-order BM-EoS are: a_0 = 13.727(10) Å, $K_{T0}(a)$ = 29(2) GPa, and $K'(a)$ = 4.9(6) for **a** axis; b_0 = 13.751(15) Å, $K_{T0}(b)$ = 20(1) GPa, and $K'(b)$ = 5.2(5) for **b**; c_0 = 13.822(31) Å, $K_{T0}(c)$ = 11(1) GPa, and $K'(c)$ = 12.6(6) for **c** [$K_{T0}(a)$:$K_{T0}(b)$:$K_{T0}(c)$ = 2.64:1.82:1.00]. The crossover between b and c EoS at P = 4.34(5) GPa (Fig. 1) is due to the larger $K'(c)$ value.

Axial and volume finite strain ($f_e = [(V_0/V)^{2/3} - 1]/2$, Angel 2000) vs. normalized stress ($F_e = P/[3f(1 + 2f)^{5/2}]$, Angel 2000) of the triclinic polymorph were calculated using the V_0, a_0, b_0, and c_0 values obtained from the BM-EoS. The fe-Fe plots are shown in Figure 2. The weighted linear regressions through the data points give: $Fe(0)$ = 19.2(2) GPa and K' = 6.5(2) for the unit-cell volume, $Fe_a(0)$ = 28.8(4) GPa and $K'(a)$ = 5.3(5) for **a**, $Fe_b(0)$ = 18.9(5) GPa and $K'(b)$ = 5.6(3) for **b**, $Fe_c(0)$ = 11.4(3) GPa and $K'(c)$ = 11.9(3) for **c**. Axial- and volume-normalized stress values extrapolated at ambient conditions [$Fe(0)$, $Fe_a(0)$, $Fe_b(0)$, $Fe_c(0)$] and the bulk modulus pressure derivatives [K', K'(a), K'(b), K'(c)], calculated on the basis of the slopes, are in agreement with the elastic parameters previously calculated with BM-EoS.

At P = 8.20(5) GPa, the gasket hole collapsed and the crystal of analcime was broken by the diamonds. A small fragment of the crystal (60 × 50 × 40 μm) was recovered from the DAC and the unit-cell constants were measured at ambient conditions, showing a metrically cubic lattice (with deviation from the cubic symmetry less than 2.5σ). The reflection conditions agreed with the $Ia\overline{3}d$ space group.

Structural evolution with pressure

The HP-crystal structure evolution of analcime was studied on the basis of six structural refinements at different pressures (Table 2), three for the low-P cubic and three for the HP-triclinic polymorph. The framework site positions obtained from refinement of the data collected with the crystal in air are in excellent agreement with those reported by Line et al. (1996)
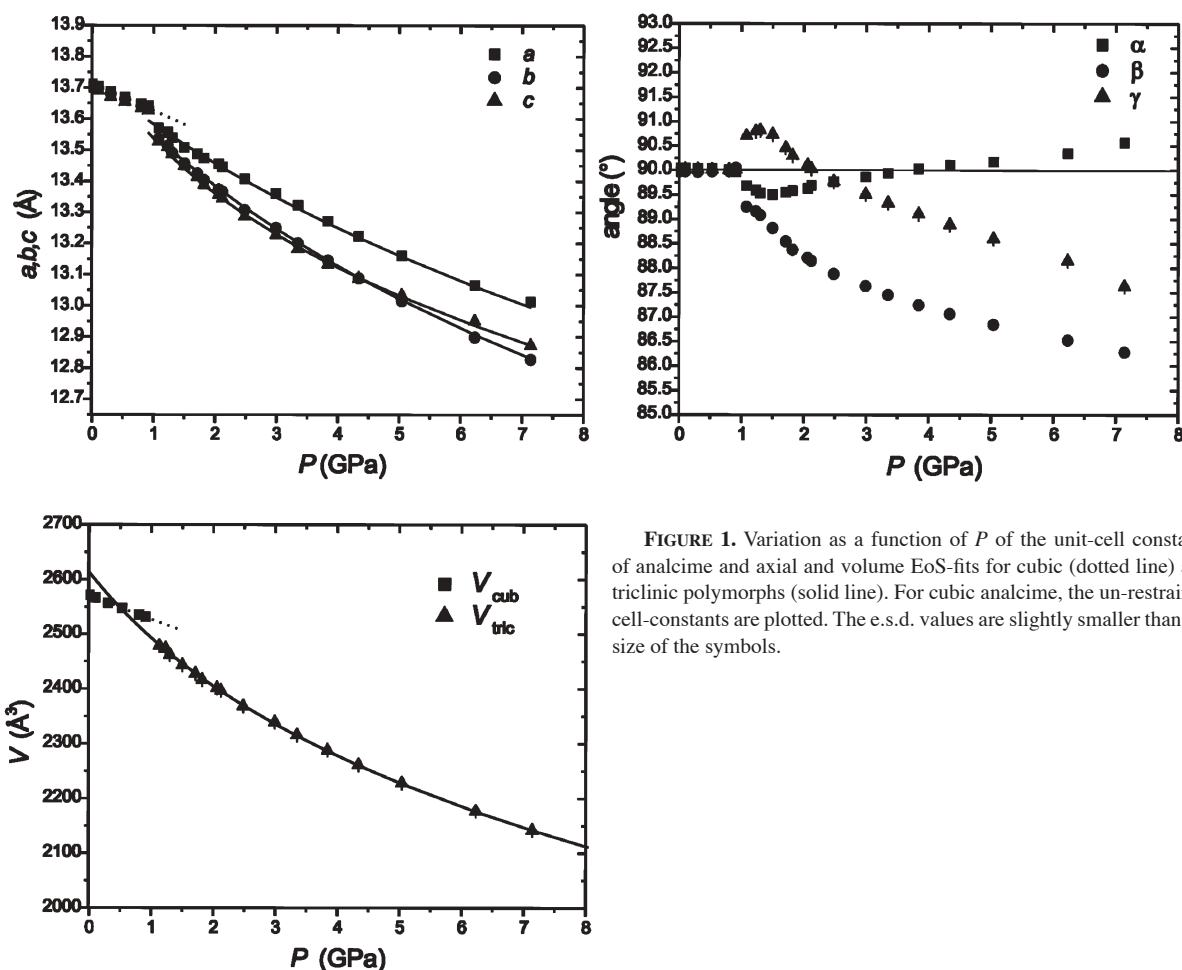
FIGURE 1. Variation as a function of *P* of the unit-cell constants of analcime and axial and volume EoS-fits for cubic (dotted line) and triclinic polymorphs (solid line). For cubic analcime, the un-restrained cell-constants are plotted. The e.s.d. values are slightly smaller than the size of the symbols.

for a synthetic cubic analcime. The fraction of sodium at the Na site was refined, resulting in a value slightly lower than the theoretical two thirds, and the refined fraction of oxygen at the W site showed full occupancy (Table 3), in agreement with the chemical analysis. A further structure refinement was performed under ambient conditions with the crystal in the DAC. The Na and W occupancies were fixed to the values obtained for the crystal in air. Only very small differences can be observed in the atomic positions and thermal displacement parameters with respect to those obtained for the crystal in air (Table 3). At 0.91(5) GPa, the crystal structure is still cubic: no evidence of violation (in terms of reflection conditions) of the $Ia\overline{3}d$ space group was observed. As expected, bond distances and thermal parameters are slightly smaller than those obtained at ambient conditions (Table 3).

The crystal structures of the HP triclinic polymorph were refined at 1.23(5), 2.12(5), and 5.04(5) GPa in the $P\overline{1}$ space group. The structural modification due to the cubic → triclinic phase transition can be deduced from Figures 3a–3b. Tetrahedral bond distances and angles show a Si/Al-statistical distribution up to the maximum pressure achieved and a strong deformation mechanism of the Na-polyhedra in response to the applied pressure (Table 5).

The main deformation mechanism of the tetrahedral framework consists of polyhedral tilting. To describe the mechanism

which acts on the tetrahedral framework, we analyzed the *P*-induced evolution of the six-membered rings lying along the [111] direction of the cubic structure (Si6-Si17-Si2-Si5-Si18-Si1, 6mR, 6 SBU, Fig. 4), and the distorted eight-membered ring (Si14-Si20-Si7-Si12-Si23-Si16-Si18-Si1, 8mR) connected to the small four-membered ring (Si9-Si14-Si1-Si6, 4mR, 4 SBU, Fig. 5). Before the cubic → triclinic phase transition, the 6mR along [111] is a perfect hexagonal ring, with a T-O-T angle of about 143.4° at 0.91(5) GPa (Table 8). At 1.23(5) GPa, the 6mR shows two different strongly deformed configurations (overlapped in Fig. 3b and defined as {1} and {2} in Fig. 4), with the T-O-T angles between 128° and 139° for configuration {1} and between 135° and 155° for configuration {2} (Table 8). In addition, the elliptic shape of the two configurations is differently oriented (Fig. 4). To quantify the evolution of the 6mR ring, the ellipticity ratios ($\varepsilon_{[6mR-1]} = 0.5\cdot[(O1-O1) + (O33-O34)]/[(O18-O17)]$ for {1}, $\varepsilon_{[6mR-2]} = 0.5\cdot[(O29-O29) + (O48-O48)]/[(O13-O13)]$ for {2}) were calculated (Fig. 4, Table 8). Both 6mR configurations show an increase in ellipticity with *P*, but configuration {2} deforms more in response to the applied pressure than configuration {1} (Table 8). The 8mR ring shows a strong deformation in response to the applied pressure. For example, between 1.23(5) and 5.04(5) GPa, the Si16-O26-Si18 and Si20-O4-Si7 angles show an increase of 7% and a decrease of 15%, respectively (Fig. 5,

TABLE 4. Refined atomic positions and displacement parameters (Å²) of high-*P* triclinic analcime. Standard deviations are in parenthesis

P (GPa)	1.23(5)				2.12(5)				5.04(5)			
	x	*y*	*z*	U_{iso}	*x*	*Y*	*z*	U_{iso}	*x*	*y*	*z*	U_{iso}
Si1	0.628(2)	0.654(4)	0.895(1)	0.0023(8)	0.629(2)	0.641(5)	0.903(2)	0.002(1)	0.632(2)	0.636(3)	0.904(1)	0.002(1)
Si2	0.876(1)	0.839(4)	0.583(1)	0.0023	0.877(2)	0.844(5)	0.577(2)	0.002	0.876(2)	0.847(4)	0.575(1)	0.002
Si3	0.849(2)	0.685(4)	0.097(2)	0.0023	0.854(2)	0.667(4)	0.101(2)	0.002	0.839(2)	0.691(4)	0.107(2)	0.002
Si4	0.625(2)	0.845(4)	0.402(1)	0.0023	0.640(2)	0.824(5)	0.385(2)	0.002	0.640(2)	0.831(4)	0.378(2)	0.002
Si5	0.889(2)	0.634(4)	0.668(2)	0.0023	0.883(2)	0.634(4)	0.663(2)	0.002	0.878(2)	0.626(4)	0.672(2)	0.002
Si6	0.607(1)	0.869(4)	0.834(2)	0.0023	0.612(2)	0.860(4)	0.815(2)	0.002	0.624(2)	0.837(3)	0.811(2)	0.002
Si7	0.580(2)	0.619(4)	0.352(1)	0.0023	0.574(2)	0.598(4)	0.348(2)	0.002	0.574(2)	0.599(4)	0.356(2)	0.002
Si8	0.915(2)	0.894(4)	0.177(1)	0.0023	0.906(2)	0.899(4)	0.163(2)	0.002	0.907(2)	0.907(4)	0.153(2)	0.002
Si9	0.621(2)	0.157(4)	1.088(2)	0.0023	0.605(2)	0.143(5)	1.082(2)	0.002	0.602(2)	0.149(4)	1.088(1)	0.002
Si10	1.104(2)	0.643(4)	0.584(2)	0.0023	1.112(2)	0.652(6)	0.604(2)	0.002	1.112(2)	0.622(5)	0.606(2)	0.002
Si11	0.880(2)	0.175(5)	0.905(2)	0.0023	0.886(2)	0.164(5)	0.919(2)	0.002	0.883(2)	0.171(4)	0.926(2)	0.002
Si12	0.629(2)	0.336(3)	0.575(1)	0.0023	0.636(2)	0.333(4)	0.579(2)	0.002	0.637(2)	0.317(4)	0.578(2)	0.002
Si13	0.084(2)	0.860(4)	0.669(1)	0.0023	0.072(2)	0.863(5)	0.659(2)	0.002	0.079(2)	0.864(4)	0.642(1)	0.002
Si14	0.586(2)	0.373(3)	1.149(1)	0.0023	0.594(2)	0.370(4)	1.157(2)	0.002	0.579(2)	0.360(3)	1.166(2)	0.002
Si15	0.418(2)	0.875(3)	1.343(2)	0.0023	0.426(2)	0.881(4)	1.335(2)	0.002	0.434(1)	0.881(3)	1.319(1)	0.002
Si16	0.938(2)	0.392(4)	0.837(2)	0.0023	0.951(2)	0.379(4)	0.820(2)	0.002	0.959(2)	0.382(3)	0.808(1)	0.002
Si17	0.672(2)	0.909(4)	0.612(2)	0.0023	0.666(2)	0.908(5)	0.607(2)	0.002	0.642(2)	0.903(4)	0.599(2)	0.002
Si18	0.851(2)	0.595(4)	0.882(2)	0.0023	0.853(2)	0.584(5)	0.886(2)	0.002	0.841(2)	0.586(4)	0.891(2)	0.002
Si19	0.851(2)	0.922(5)	0.377(2)	0.0023	0.859(2)	0.918(5)	0.368(2)	0.002	0.863(2)	0.918(4)	0.368(2)	0.002
Si20	0.629(2)	0.608(4)	1.114(2)	0.0023	0.628(2)	0.594(5)	1.121(2)	0.002	0.622(2)	0.582(4)	1.129(2)	0.002
Si21	0.681(2)	0.421(4)	0.356(2)	0.0023	0.682(2)	0.391(5)	0.362(2)	0.002	0.681(2)	0.387(4)	0.365(2)	0.002
Si22	0.817(2)	1.098(4)	1.123(2)	0.0023	0.818(2)	1.099(6)	1.148(2)	0.002	0.807(2)	1.137(5)	1.157(2)	0.002
Si23	0.823(2)	0.416(5)	0.634(2)	0.0023	0.831(2)	0.420(5)	0.621(2)	0.002	0.829(2)	0.416(5)	0.624(2)	0.002
Si24	0.339(2)	0.909(5)	1.134(2)	0.0023	0.319(2)	0.926(5)	1.141(2)	0.002	0.312(2)	0.939(4)	1.134(2)	0.002
O1	0.625(4)	0.849(6)	0.713(3)	0.006(1)	0.615(5)	0.837(7)	0.697(3)	0.005(1)	0.629(4)	0.818(6)	0.687(3)	0.004(1)
O2	0.894(4)	0.659(6)	0.789(2)	0.006	0.885(5)	0.649(7)	0.784(3)	0.005	0.894(4)	0.658(6)	0.795(3)	0.004
O3	0.926(4)	0.881(7)	0.298(3)	0.006	0.930(4)	0.872(7)	0.280(3)	0.005	0.938(3)	0.885(7)	0.270(4)	0.004
O4	0.582(4)	0.626(7)	1.229(2)	0.006	0.555(4)	0.602(9)	1.226(3)	0.005	0.546(3)	0.596(7)	1.235(2)	0.004
O5	0.369(4)	0.634(7)	0.738(3)	0.006	0.368(4)	0.664(7)	0.732(3)	0.005	0.374(4)	0.671(6)	0.724(3)	0.004
O6	0.887(4)	0.151(7)	1.213(3)	0.006	0.894(4)	0.147(8)	1.222(3)	0.005	0.897(4)	0.165(7)	1.236(3)	0.004
O7	1.107(4)	0.626(8)	0.277(3)	0.006	1.094(4)	0.620(8)	0.292(3)	0.005	1.083(3)	0.633(7)	0.309(3)	0.004
O8	0.416(4)	0.868(7)	1.219(2)	0.006	0.398(4)	0.871(7)	1.215(3)	0.005	0.387(3)	0.871(6)	1.207(3)	0.004
O9	0.608(4)	0.859(7)	0.525(3)	0.006	0.625(5)	0.848(8)	0.505(3)	0.005	0.606(4)	0.859(7)	0.492(3)	0.004
O10	0.863(4)	0.667(6)	0.978(3)	0.006	0.888(5)	0.644(7)	0.986(3)	0.005	0.882(4)	0.652(7)	0.992(3)	0.004
O11	0.894(4)	0.854(7)	0.466(3)	0.006	0.925(5)	0.881(8)	0.468(3)	0.005	0.912(3)	0.835(6)	0.449(3)	0.004
O12	0.586(3)	0.643(7)	1.007(2)	0.006	0.593(4)	0.656(7)	1.021(3)	0.005	0.572(3)	0.624(7)	1.023(3)	0.004
O13	0.347(4)	0.646(6)	0.544(3)	0.006	0.328(4)	0.682(6)	0.538(3)	0.005	0.314(3)	0.696(5)	0.542(3)	0.004
O14	0.856(4)	0.154(7)	1.022(3)	0.006	0.856(4)	0.160(8)	1.042(3)	0.005	0.840(4)	0.191(7)	1.044(3)	0.004
O15	1.120(4)	0.612(8)	0.469(3)	0.006	1.112(4)	0.612(8)	0.484(4)	0.005	1.130(4)	0.568(7)	0.494(3)	0.004
O16	0.391(4)	0.883(7)	1.026(3)	0.006	0.368(4)	0.909(8)	1.026(3)	0.005	0.357(4)	0.909(6)	1.019(3)	0.004
O17	0.726(3)	0.583(6)	0.884(4)	0.006	0.730(3)	0.571(6)	0.901(4)	0.005	0.724(2)	0.553(5)	0.891(4)	0.004
O18	0.787(3)	0.908(6)	0.631(4)	0.006	0.784(3)	0.914(7)	0.619(4)	0.005	0.770(3)	0.917(6)	0.587(4)	0.004
O19	0.745(3)	0.628(7)	1.131(4)	0.006	0.740(3)	0.638(8)	1.135(4)	0.005	0.732(3)	0.637(7)	1.145(4)	0.004
O20	0.733(3)	0.887(7)	0.359(4)	0.006	0.739(3)	0.888(7)	0.343(4)	0.005	0.750(3)	0.877(7)	0.335(4)	0.004
O21	0.707(3)	0.109(7)	1.155(3)	0.006	0.695(3)	0.116(9)	1.162(4)	0.005	0.685(3)	0.138(7)	1.179(3)	0.004
O22	1.196(3)	0.584(7)	0.644(3)	0.006	1.195(3)	0.595(8)	0.661(5)	0.005	1.201(3)	0.587(8)	0.672(4)	0.004
O23	0.778(3)	0.122(7)	0.863(3)	0.006	0.794(4)	0.124(8)	0.860(4)	0.005	0.803(3)	0.105(7)	0.867(4)	0.004
O24	0.713(3)	0.362(7)	0.660(3)	0.006	0.724(4)	0.368(8)	0.654(4)	0.005	0.723(3)	0.358(7)	0.652(3)	0.004
O25	0.361(4)	0.974(4)	1.380(4)	0.006	0.378(4)	0.981(4)	1.388(5)	0.005	0.402(4)	0.988(4)	1.380(4)	0.004
O26	0.882(4)	0.479(4)	0.897(4)	0.006	0.904(4)	0.473(5)	0.890(4)	0.005	0.925(3)	0.489(4)	0.871(4)	0.004
O27	0.859(4)	1.043(4)	0.389(4)	0.006	0.865(5)	1.039(5)	0.379(5)	0.005	0.853(4)	1.040(4)	0.402(4)	0.004
O28	0.621(4)	0.482(4)	1.097(4)	0.006	0.640(4)	0.472(5)	1.105(5)	0.005	0.642(4)	0.459(4)	1.120(4)	0.004
O29	0.656(4)	0.534(4)	0.389(4)	0.006	0.640(4)	0.503(5)	0.382(5)	0.005	0.642(4)	0.504(4)	0.399(4)	0.004
O30	0.857(4)	0.986(4)	0.132(3)	0.006	0.838(4)	0.984(5)	0.117(5)	0.005	0.837(4)	1.011(4)	0.142(4)	0.004
O31	0.815(4)	0.539(5)	0.635(4)	0.006	0.824(4)	0.538(5)	0.626(4)	0.005	0.804(4)	0.532(4)	0.669(4)	0.004
O32	0.665(4)	0.968(4)	0.872(4)	0.006	0.686(4)	0.952(5)	0.847(4)	0.005	0.694(4)	0.938(4)	0.836(4)	0.004
O33	0.839(4)	0.726(4)	0.608(4)	0.006	0.839(5)	0.727(5)	0.595(4)	0.005	0.848(4)	0.733(4)	0.617(4)	0.004
O34	0.659(4)	0.772(4)	0.883(4)	0.006	0.654(5)	0.763(5)	0.882(4)	0.005	0.673(4)	0.754(4)	0.893(4)	0.004
O35	0.622(4)	0.725(4)	0.395(3)	0.006	0.643(4)	0.702(5)	0.365(4)	0.005	0.645(4)	0.704(4)	0.364(4)	0.004
O36	0.858(4)	0.798(4)	0.134(4)	0.006	0.870(5)	0.791(4)	0.111(4)	0.005	0.841(4)	0.816(4)	0.105(4)	0.004
O37	1.123(4)	0.763(4)	0.606(4)	0.006	1.114(5)	0.771(5)	0.590(5)	0.005	1.093(4)	0.749(4)	0.591(4)	0.004
O38	0.620(4)	0.279(4)	1.079(4)	0.006	0.606(5)	0.268(5)	1.085(5)	0.005	0.597(4)	0.277(4)	1.066(3)	0.004
O39	0.591(4)	0.221(4)	0.583(3)	0.006	0.621(4)	0.212(4)	0.599(4)	0.005	0.626(4)	0.195(4)	0.601(3)	0.004
O40	0.884(4)	0.296(5)	0.897(4)	0.006	0.918(4)	0.279(5)	0.887(4)	0.005	0.914(4)	0.286(5)	0.881(4)	0.004
O41	0.532(3)	0.624(7)	0.826(3)	0.006	0.528(3)	0.611(8)	0.845(4)	0.005	0.544(2)	0.614(7)	0.824(3)	0.004
O42	0.963(3)	0.872(7)	0.662(3)	0.006	0.952(3)	0.865(9)	0.672(3)	0.005	0.962(3)	0.905(6)	0.642(3)	0.004
O43	1.062(3)	0.381(6)	0.846(3)	0.006	1.071(3)	0.394(7)	0.822(4)	0.005	1.081(3)	0.345(7)	0.805(3)	0.004
O44	0.536(2)	0.908(5)	0.359(4)	0.006	0.550(4)	0.884(7)	0.329(4)	0.005	0.561(2)	0.885(7)	0.298(4)	0.004
O45	0.484(2)	0.877(7)	0.853(3)	0.006	0.505(3)	0.893(7)	0.870(4)	0.005	0.503(3)	0.875(6)	0.848(4)	0.004
O46	0.997(3)	0.604(7)	0.628(4)	0.006	1.005(3)	0.602(8)	0.646(4)	0.005	0.994(3)	0.575(6)	0.645(4)	0.004
O47	1.031(3)	0.888(7)	0.138(3)	0.006	1.018(3)	0.911(7)	0.108(4)	0.005	1.015(3)	0.907(7)	0.080(4)	0.004
O48	0.532(3)	0.405(5)	0.604(3)	0.006	0.534(3)	0.403(7)	0.584(4)	0.005	0.532(3)	0.383(6)	0.576(4)	0.004
W1	0.603(7)	0.650(14)	0.607(6)	0.047(6)	0.586(8)	0.585(21)	0.607(9)	0.04(2)	0.590(7)	0.582(14)	0.616(7)	0.04(1)
W2	1.099(7)	1.079(14)	0.119(6)	0.047	1.099(8)	1.107(20)	0.113(10)	0.04	1.089(7)	1.121(15)	0.099(7)	0.04

Note: For all of the Si, O, and W sites the occupancy was fixed at 1/1, whereas the Na sites were fixed at 0.570 (see text and Table 3).

TABLE 4.—*Continued.*

P (GPa)	1.23(5)				2.12(5)				5.04(5)			
	x	y	z	U_{iso}	x	Y	z	U_{iso}	x	y	z	U_{iso}
W3	0.867(6)	0.637(15)	0.369(6)	0.047	0.893(8)	0.623(19)	0.388(7)	0.04	0.911(6)	0.605(16)	0.402(6)	0.04
W4	0.606(6)	0.880(14)	1.109(6)	0.047	0.617(8)	0.872(18)	1.087(2)	0.04	0.614(7)	0.860(16)	1.081(7)	0.04
W5	0.385(7)	0.921(14)	0.637(6)	0.047	0.379(9)	0.913(17)	0.634(9)	0.04	0.393(7)	0.909(15)	0.635(6)	0.04
W6	0.874(6)	0.359(14)	1.134(6)	0.047	0.884(9)	0.395(19)	1.131(9)	0.04	0.889(7)	0.406(16)	1.116(7)	0.04
W7	1.158(7)	0.843(15)	0.357(7)	0.047	1.162(9)	0.843(22)	0.365(9)	0.04	1.159(7)	0.856(16)	0.373(7)	0.04
W8	0.654(7)	0.380(16)	0.861(7)	0.047	0.655(9)	0.366(22)	0.863(9)	0.04	0.658(7)	0.334(14)	0.861(7)	0.04
Na1	0.631(5)	0.499(13)	0.729(5)	0.047	0.550(6)	0.488(14)	0.717(6)	0.04	0.582(5)	0.453(9)	0.755(5)	0.04
Na2	1.145(5)	0.965(11)	0.274(5)	0.047	1.123(6)	0.978(13)	0.256(6)	0.04	1.134(6)	1.007(12)	0.245(5)	0.04
Na3	0.864(5)	0.484(12)	0.229(5)	0.047	0.855(6)	0.502(11)	0.238(6)	0.04	0.906(5)	0.504(9)	0.215(5)	0.04
Na4	0.588(5)	0.991(12)	1.213(5)	0.047	0.579(5)	0.966(11)	1.222(5)	0.04	0.653(5)	0.985(9)	1.196(5)	0.04
Na5	0.735(7)	0.625(16)	0.495(6)	0.047	0.750(8)	0.634(21)	0.498(8)	0.04	0.750(7)	0.627(17)	0.504(7)	0.04
Na6	0.767(6)	0.849(15)	0.997(6)	0.047	0.768(9)	0.861(21)	1.002(8)	0.04	0.759(7)	0.875(17)	0.998(7)	0.04
Na7	0.263(7)	0.860(16)	0.501(6)	0.047	0.266(9)	0.892(24)	0.504(9)	0.04	0.267(7)	0.867(17)	0.500(7)	0.04
Na8	0.763(7)	0.353(16)	1.002(6)	0.047	0.768(9)	0.345(24)	0.998(9)	0.04	0.766(7)	0.384(17)	0.997(7)	0.04
Na9	0.483(6)	0.771(14)	0.618(6)	0.047	0.496(7)	0.764(18)	0.621(8)	0.04	0.496(6)	0.746(15)	0.605(6)	0.04
Na10	0.996(6)	0.258(14)	1.121(6)	0.047	0.991(7)	0.268(17)	1.111(8)	0.04	0.983(6)	0.269(15)	1.113(7)	0.04
Na11	1.017(6)	0.742(14)	0.384(6)	0.047	1.030(9)	0.769(18)	0.396(9)	0.04	1.037(6)	0.745(15)	0.389(6)	0.04
Na12	0.492(7)	0.754(15)	1.118(6)	0.047	0.476(9)	0.736(18)	1.117(9)	0.04	0.475(6)	0.737(14)	1.096(6)	0.04

Note: For all of the Si, O, and W sites the occupancy was fixed at 1/1, whereas the Na sites were fixed at 0.570 (see text and Table 3).
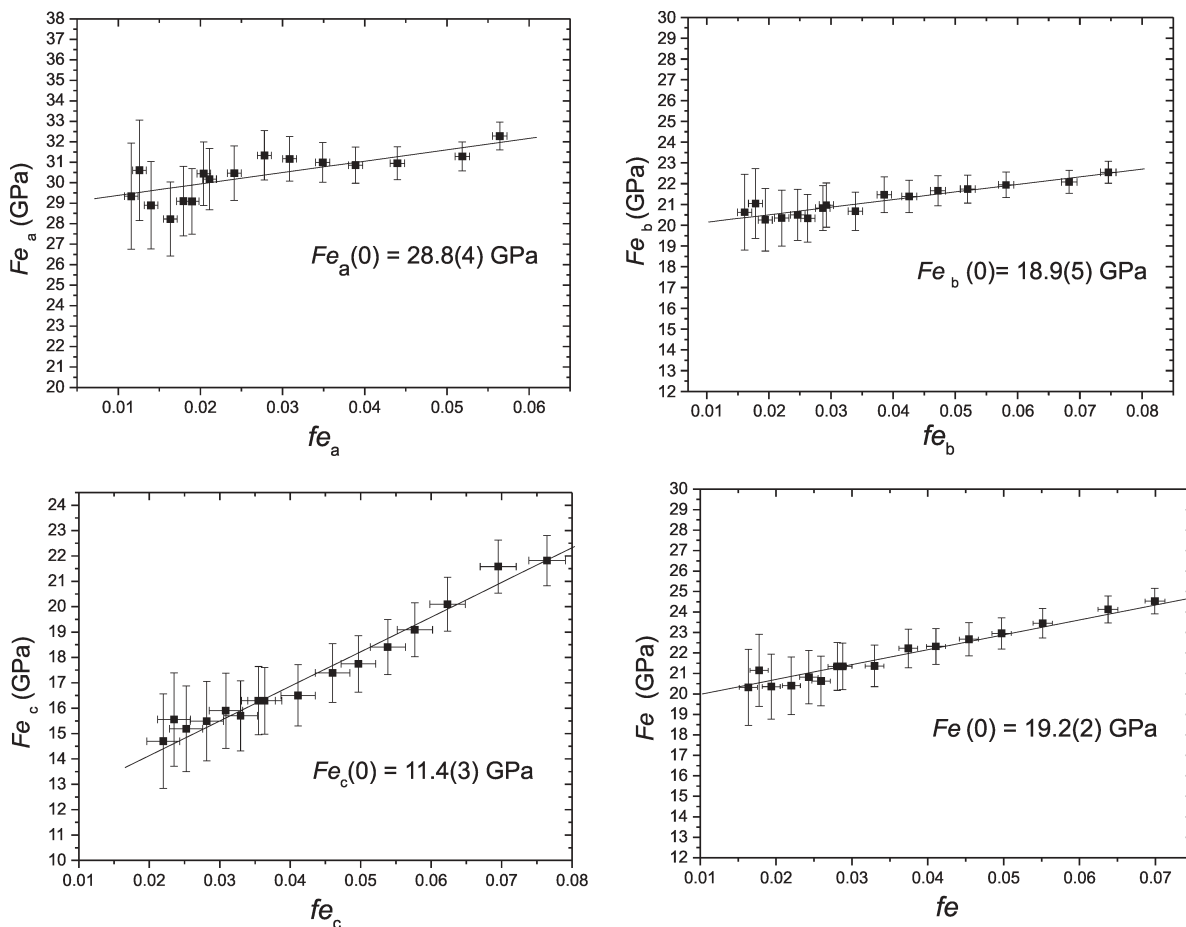

FIGURE 2. Plot of the axial and volume finite strain (f_e) vs. the normalized stress (F_e) for triclinic analcime, calculated using the a_0, b_0, c_0, and V_0 values obtained from the third-order BM-EoS (see text). The e.s.d. values were calculated according to Heinz and Jeanloz (1984). The weighted linear regressions through the data points are shown.

Table 8). The 4mR SBU connected to the 8mR is also deformed under HP (Table 8). The ellipticity ratio, here defined as ε_{4mR} = [O45-O41]/[O38-O34], is 0.92 at 1.23(5) GPa, 1.08 at 2.12(5) GPa, and 0.96 at 5.04(5) GPa.

In the cubic structure, the Na sites are six-coordinated (four O

atoms belonging to the tetrahedral framework and 2 water molecules, Table 3). At *P* above the cubic → triclinic phase transition, the topological configuration of the extra-framework content appears to change. At 1.23(5) GPa, the structural refinement shows that eight Na sites have a coordination number CN = 6 and four

FIGURE 3. Structural modification induced by the first order phase transition from cubic (top) to triclinic (bottom) analcime, (**a**) viewed along [100] and (**b**) along the cubic [111]. For the extra-framework content, the large spheres represent the Na sites, whereas the small spheres represent the W sites.

Na sites have a CN = 7 (Table 6). At 2.12(5) GPa six Na sites show CN = 6 and six Na sites CN = 7 (Table 6). At 5.04(5) GPa, four Na sites show CN = 6, seven Na sites CN = 7, and one Na site CN = 8 (Table 6). Although the atomic positions of the extra-framework cations should be considered simply the "most probable" site positions, due to the refinement procedure adopted, the structural changes of the topological configuration of the extra-framework content appear to be consistent. On the basis of the final difference-Fourier map of the HP-refinements, we can exclude any *P*-induced over-hydration effect through the selective sorption of water molecules from the hydrous *P*-fluid used in this experiment. In addition, the *P*-induced over-hydration effects observed for other microporous materials give rise to a first-order phase-transition with increase of the unit-cell volume (Lee et al. 2002a, b, 2004a). Such a behavior is not observed for analcime.

DISCUSSION AND CONCLUSIONS

Analcime is the first open framework silicate, belonging to the ANA group (Armbruster and Gunter 2001; Baerlocher et al. 2001) investigated up to 7.14(5) GPa. Only one phase transition from cubic to triclinic symmetry was observed. No evidence of an intermediate monoclinic phase, like that suggested by Hazen and Finger (1979), has been found. In fact, above 1.08(5) GPa all angles deviate significantly from 90°. Although we observed a change in the behavior of the angles with *P* at about 1.3-1.5 GPa, this is smooth and does not give rise to any appreciable discontinuity in the axial and volume behavior like those suggested by Hazen and Finger (1979) (Fig. 1, Table 1). A non-monotonic trend of the angle values with *P* has been observed for other framework silicates without implying any phase transition (Allan and Angel 1997; Tribaudino et al. 1999; Benusa et al. 2005). On the basis of the structural refinements, we can confirm that the cubic to triclinic phase transition is displacive in character
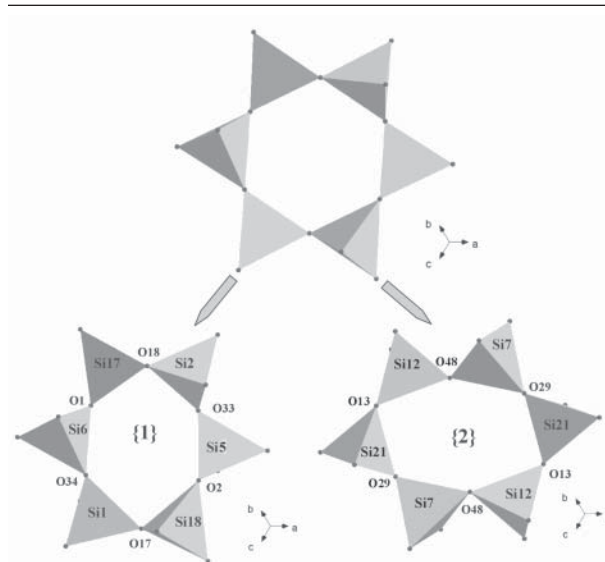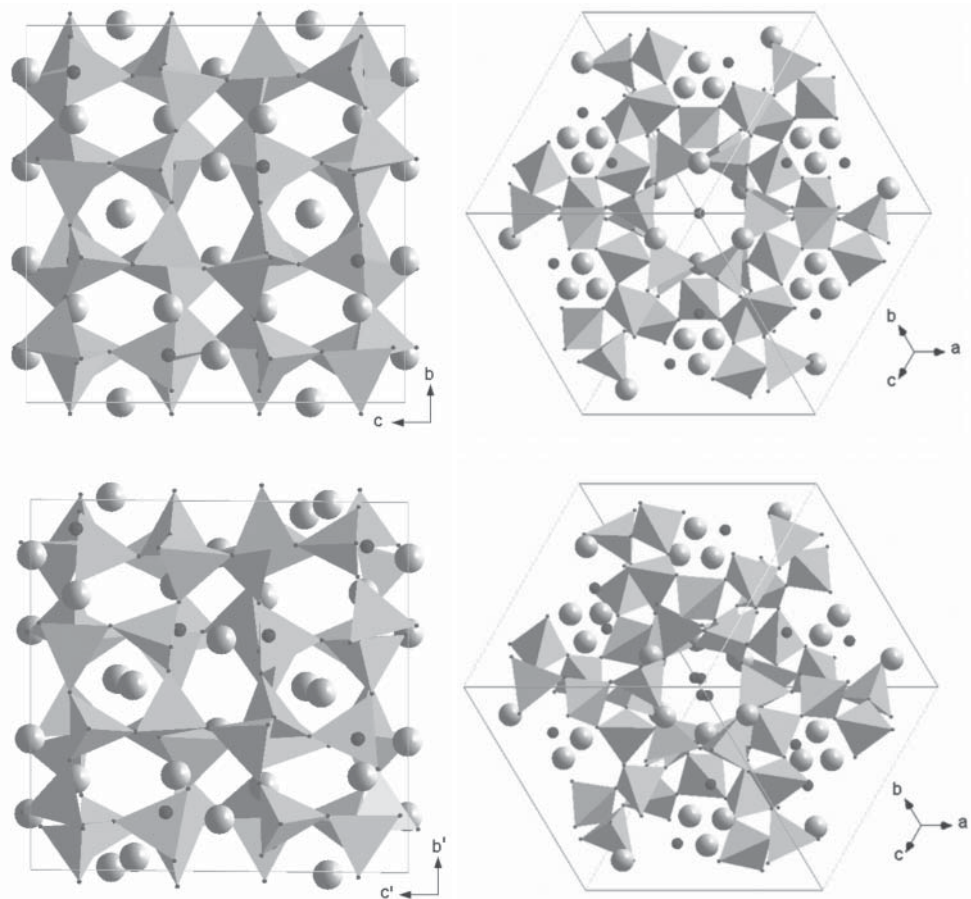
FIGURE 4. Structural modification induced by the first order phase transition from cubic to triclinic analcime on 6mR along the cubic [111] direction. Before the phase transition, 6mR is a perfect hexagonal ring (above). After the phase transition, the 6mR ring shows two different strongly deformed configurations: {1} and {2} (below). Configuration {2} lies on the inversion center.
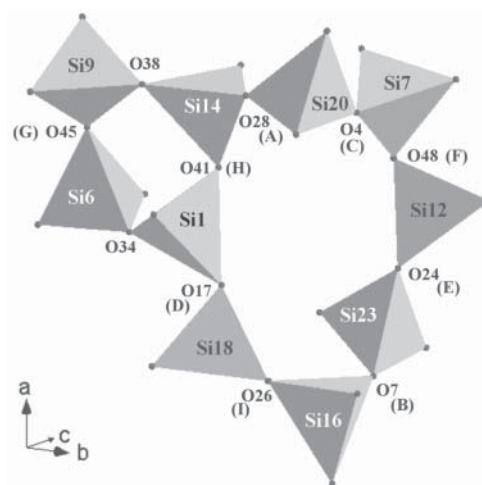
TABLE 8. Selected structural parameters of cubic and triclinic anal-cime at different pressures

P (GPa)	0.0001	0.0001*	0.91(5)	1.23(5)	2.12(5)	5.04(5)
six-ring {1}						
O-O	5.171(3)	5.161(8)	5.140(10)			
O1-O2				5.46(4)	4.59(6)	4.32(8)
O33-O34				4.51(5)	4.53(6)	4.17(6)
O17-O18				5.59(6)	5.94(7)	6.20(9)
ε (6mR-1)	1	1	1	0.81	0.77	0.68
Si-O-Si	144.79(9)	143.7(6)	143.4(7)			
Si6-O1-Si17				138.6(31)	125.9(35)	127.0(37)
Si17-O18-Si2				131.7(36)	134.4(38)	140.3(41)
Si2-O33-Si5				132.6(33)	132.2(29)	151.6(45)
Si5-O2-Si18				128.2(26)	137.5(35)	120.0(27)
Si18-O17-Si1				138.7(42)	139.1(33)	121.3(31)
Si1-O34-Si6				138.5(37)	139.9(40)	121.7(33)
six-ring {2}						
O-O	5.171(3)	5.161(8)	5.140(10)			
O13-O13				5.89(3)	6.76(5)	7.04(6)
O29-O29				5.22(4)	4.82(4)	4.45(4)
O48-O48				3.91(2)	3.57(4)	3.74(5)
ε (6mR-2)	1	1	1	0.77	0.62	0.58
Si-O-Si	144.79(9)	143.7(6)	143.4(7)			
Si21-O13-Si12 (×2)				154.8(41)	135.3(28)	126.6(31)
Si12-O48-Si7 (×2)				134.1(33)	135.9(35)	140.5(43)
Si7-O29-Si21 (×2)				135.5(34)	150.1(47)	139.6(35)
four-ring SBU						
O-O	3.772(2)	3.801(7)	3.784(9)			
O41-O45				3.51(2)	3.80(3)	3.44(5)
O34-O38				3.81(3)	3.53(5)	3.58(6)
ε (4mR)	1	1	1	0.92	1.08	0.96
Si-O-Si	144.79(9)	143.7(6)	143.4(7)			
Si9-O38-Si14				137.8(28)	145.7(42)	119.8(28)
Si14-O41-Si1				130.3(35)	143.2(38)	130.2(35)
Si1-O34-Si6				138.5(39)	139.9(35)	121.7(38)
Si6-O45-Si9				156.4(41)	147.2(40)	148.8(47)
eight-ring						
O-O (B-C, A-I)	6.913(3)	6.906(8)	6.872(11)			
O4-O7				6.47(4)	6.23(6)	6.12(6)
O26-O28				6.84(6)	7.35(8)	7.46(8)
O-O (D-E, F-H)	4.290(2)	4.248(6)	4.225(8)			
O17-O24				4.27(3)	4.28(5)	4.01(6)
O41-O48				4.23(4)	4.46(3)	4.42(5)
O-O (C-I)	6.618(3)	6.599(9)	6.556(10)			
O26-O4				6.67(5)	6.49(5)	6.53(7)
Si-O-Si	144.79(9)	143.7(6)	143.4(7)			
Si14-O28-Si20				144.9(42)	136.7(35)	132.9(37)
Si20-O4-Si7				155.6(35)	135.0(38)	129.8(26)
Si7-O48-Si12				134.1(29)	135.9(37)	140.4(44)
Si12-O24-Si23				123.2(28)	127.3(29)	130.4(32)
Si23-O7-Si16				146.4(34)	153.5(46)	137.4(36)
Si16-O26-Si18				139.9(40)	144.3(40)	149.2(45)
Si18-O17-Si1				138.6(31)	138.9(37)	121.3(27)
Si-Si	7.917(3)	7.891(8)	7.853(9)			
Si20-Si16				7.70(6)	7.80(8)	7.64(7)
O-O	11.132(5)	11.124(10)	11.086(13)			
O19-O43				10.94(8)	10.90(9)	10.66(11)
O-O-O (G-H-F)	136.2(1)	136.2(4)	136.2(5)			
O45-O41-O48				139.5(36)	133.7(30)	136.4(41)

* Data collected with the crystal in the DAC without P-medium
Notes: ε(6mR-1) = 0.5·[(O1-O1) + (O33-O34)]/[(O18-O17)], ε(6mR-2) = 0.5·[(O29-O29) + (O48-O48)]/[(O13-O13)], ε(4mR) = [O45-O41]/[O38-O34] (see text and Fig. 4 and 5); e.s.d. values of ε(6mR-1), ε(6mR-2), and ε(4mR) are less than 0.02

FIGURE 5. Topological configuration of the distorted 8mR ring (Si14-Si20-Si7-Si12-Si23-Si16-Si18-Si1, in triclinic analcime) connected to the 4mR ring (Si9-Si14-Si1-Si6, 4 SBU).

However, to our knowledge, the bulk modulus value obtained for triclinic analcime is the lowest reported in the literature for natural open-framework silicates.

The structural refinements performed at HP enable us to understand the reason for the elastic anisotropy of the triclinic polymorph and the main deformation mechanisms of framework and extra-framework content. The distorted 6mR ring (lying along the cubic [111] direction), shows two differently oriented configurations, {1} and {2}, which increase their ellipticity with P (Fig. 4). However, configuration {2} becomes more elliptic in response to the applied pressure than configuration {1} (Fig. 4, Table 8). This effect gives rise to lower compressibility along **a** than along **b** or **c** axis [i.e., $K_{T0}(a)$ higher than $K_{T0}(b)$ or $K_{T0}(c)$]. In addition, the non-monotonic behavior observed for the α, β, and γ angles with P (Fig. 1, Table 1), can be explained to a first approximation by the change in the evolution of several structural parameters of the framework. For example, if we consider configuration {2}, the structural refinements at P > 1.23(5) GPa show that the Si7-O29-Si21 angle first increases [+10% between 1.23(5) and 2.12(5) GPa] and then decreases [–7% between 2.23(5) and 5.04(5) GPa, Table 8] with P. Several T-O-T angles show such an oscillatory behavior: all four angles belonging to the 4mR SBU, one belonging to 8mR, and four belonging to 6mR {1} (Table 8). In addition, the kink of the connected 4mR SBU and 8mR (Fig. 5, Table 8) also shows an oscillatory behavior. In fact, the O45-O41-O48 angle first decreases [– 4% between 1.23(5) and 2.12(5) GPa] and then increases with P [+ 2% between 2.23(5) and 5.04(5) GPa, Table 8]. This suggests that there is a change in the compressional mechanism of the triclinic structure, probably at P ~ 1.3 GPa, where the change in the angles evolution is visible (Fig. 1).

The HP-structural refinements also show variation of the T-O-T angles of the 4mR SBU: the four T-O-T angles show an oscillatory behavior with P and at 5.04(5) GPa two of them (Si9-O38-Si14 and Si1-O34-Si6) decrease to values close to 120° (Table 8). The fact that this small SBU is not completely rigid with P has also been found using HP-Raman spectroscopy

and it is basically driven by tetrahedral tilting, as assumed by Hazen and Finger (1979). The triclinic polymorph shows a bulk modulus which is three times smaller than that of the low-P cubic polymorph. An increase in compressibility of the HP polymorph with respect to the low-P one has already been observed for sheet silicates (Welch et al. 2004) and carbonates (Merrill and Bassett 1972, 1975; Singh and Kennedy 1974; Martinez et al. 1996; Smyth and Ahrens 1997; Redfern 2000; Holl et al. 2000).

(Miroshnichenko and Goryainov 2000).

Some T-O-T angles have values close to the critical value of $120 \pm 3°$ at 5.04(5) GPa (Table 8). Similar values were reported for other open framework silicates under extreme conditions. Gibbs et al. (2000) calculated the theoretical elastic and structural behavior of coesite ($K_{T0} = 87.3$ GPa, $K' = 4.5$) up to ~17.4 GPa. At this P value, with $V_P-V_{P0} = -13.4\%$, the authors obtained one Si-O-Si angle of ~124°. A similar value (Si-O-Si ~ 123°) was calculated for low-quartz ($K_{T0} = 34.8$ GPa, $K' = 4.9$) at 18.7 GPa (Gibbs et al. 1999). Considering that for analcime $V_{5.04}-V_{P0} = -13.3\%$, we could prudently infer that the refined T-O-T values at 5.04(5) GPa reflect the structural assets of other less compressible framework silicates at higher pressures. However, synthetic lithium feldspar ($LiAlSi_3O_8$) shows one T-O-T angle of about 124.9° at ambient conditions (Baur et al. 1996). In addition, Benusa et al. (2005) recently reported HP structural data for low-albite with one T-O-T angle of 119.4(4)° at 6.49 GPa that decreases down to 113.7(3)° at 9.43 GPa (implying a T-T distance < 2.8 Å). Such results demonstrate the extreme flexibility of Si/Al-framework silicates under different P-T-X conditions, as emphasized by Baur et al. (1996), Ross (2000), and Gatta et al. (2003). On this basis, we cannot exclude that for the HP triclinic form of analcime the extra-framework content plays an important role, concurring to stabilize an energetically favorable topological configuration with critically low T-O-T angle values.

As expected, the strong P-induced deformation of the Si/Al-framework into the triclinic structure gives rise to a reduction of the free volume of the voids. As a consequence, the topological configuration of the extra-framework content changes: the refined positions of the Na sites show an increase in coordination number with P (Table 6).

The effect of pressure on the structural evolution of analcime appears to be more dramatic than that of temperature. In fact, at LT cubic analcime is stable at least down to 30 K and shows only a slight deformation of the crystal structure, with the T-O-T angle staying almost constant (~145°) down to the lowest T achieved (Line at al. 1996). At HT, tetragonal analcime shows a complete loss of water at 650 K (Cruciani and Gualtieri 1999). The tetragonal lattice is maintained and no phase transition is observed at least up to about 1000 K, where some evidence of evolution toward the cubic structure is reported. Despite the change of the topological configuration of the extra-framework content (due to the dehydration process), the lowest T-O-T angle observed is ~132° at 921 K, showing that the general aspect of the Si/Al-framework is well preserved. Analcime shows, therefore, a different behavior with respect to the other open framework silicates with zeolitic structures previously studied both at HT and HP. In fact, for the latter the effects of P are less dramatic than those induced by T (Comodi et al. 2001, 2002, 2003; Gatta and Wells 2004; Gatta et al. 2003, 2004a, b, 2005; Lee et al. 2002a, b, 2004a, b).

Acknowledgments

References cited

Allan, D.R. and Angel, R.J. (1997) A high-pressure structural study of microcline ($KAlSi_3O_8$) to 7 GPa. European Journal of Mineralogy, 9, 263–275.

Allan, D.R., Miletich, R., and Angel, R.J. (1996) A diamond-anvil cell for single-crystal X-ray diffraction studies to pressures in excess of 10 GPa. Review of Scientific Instruments, 67, 840–842.

Angel, R.J. (2000) Equation of state. In R.M. Hazen and R.T. Downs, Eds., High-Temperature and High-Pressure Crystal Chemistry. Reviews in Mineralogy and Geochemistry, 41, 35–59. Mineralogical Society of America and Geochemical Society, Washington, U.S.A.

——— (2001) EOS-FIT V6.0. Computer program. Crystallography Laboratory, Deparment of Geological Sciences, Virginia Tech, Blacksburg, U.S.A.

——— (2002) ABSORB V5.2. Computer program. Crystallography Laboratory, Department of Geological Sciences, Virginia Tech, Blacksburg, U.S.A.

——— (2003a) Automated profile analysis for single-crystal diffraction data. Journal of Applied Crystallography, 36, 295–300.

——— (2003b) WIN-INTEGRSTP V3.4. Computer program. Crystallography Laboratory, Department of Geological Sciences, Virginia Tech, Blacksburg, U.S.A.

Angel, R.J., Downs, R.T., and Finger, L.W. (2000) High-Temperature - High-Pressure Diffractometry. In R.M. Hazen and R.T. Downs, Eds., High-Temperature and High-Pressure Crystal Chemistry. Reviews in Mineralogy and Geochemistry, 41, 559–596. Mineralogical Society of America and Geochemical Society, Washington, U.S.A.

Armbruster, T. and Gunter, M.E. (2001) Crystal structures of natural zeolites. In D.L. Bish and D.W. Ming, Eds., Natural zeolites: Occurrence, properties, application. Reviews in Mineralogy and Geochemistry, 45, 1–57. Mineralogical Society of America and Geochemical Society, Washington, U.S.A.

Baerlocher, Ch., Meier, W.M., and Olson, D.H. (2001) Atlas of zeolite framework types, 5th ed., 302 p. Elsevier, Amsterdam, NL.

Baur, W.H., Joswig, W., and Müller, G. (1996) Mechanisms of the feldspar framework: Crystal structure of Li-feldspar. Journal of Solid State Chemistry, 12, 12–23.

Benusa, M.T., Angel, R.J., and Ross, N.L. (2005) Compression of albite, $NaAlSi_3O_8$. American Mineralogist, 90, 1115–1120.

Birch, F. (1947) Finite elastic strain of cubic crystal. Physical Review, 71, 809–824.

Burnham, C.W. (1966) Computation of absorption corrections and the significance of end effects. American Mineralogist, 51, 159–167.

Cheng, X., Zhao, P.D., and Stebbins, J.F. (2000) Solid state NMR study of oxygen site exchange and Al-O-Al site concentration in analcime. American Mineralogist, 85, 1030–1037.

Comodi, P., Gatta, G.D., and Zanazzi, P.F. (2001) High-pressure structural behavior of heulandite. European Journal of Mineralogy, 13, 497–505.

——— (2002) High-pressure behavior of scolecite. European Journal of Mineralogy, 14, 567–574.

——— (2003) Effects of pressure on the structure of bikitaite. European Journal of Mineralogy, 15, 247–225.

Coombs, D.S. (1955) X-ray investigation on wairakite and non-cubic analcime. Mineralogical Magazine, 30, 699–708.

Coombs, D.S., Alberti, A., Armbruster, T., Artioli, G., Colella, C., Galli, E., Grice, J.D., Liebau, F., Mandarino, J.A., Minato, H., Nickel, E.H., Passaglia, E., Peacor, D.R., Quartieri, S., Rinaldi, R., Ross, M., Sheppard, R.A., Tillmanns, E., and Vezzalini, G. (1997) Recommended nomenclature for zeolite minerals: Report of the Subcommittee on Zeolites of International Mineralogical Association, Commission on New Minerals and Minerals Names. Canadian Mineralogist, 35, 1571–1606.

Cruciani, G. and Gualtieri, A. (1999) Dehydration dynamics of analcime by in situ synchrotron powder diffraction. American Mineralogist, 84, 112–119.

Ferraris, G., Jones, D.W., and Yerkess, J. (1972) A neutron-diffraction study of the crystal structure of analcime, $NaAlSi_2O_6 \cdot H_2O$. Zeitschrift fuer Kristallographie, 135, 240–252.

Gatta, G.D. and Boffa Ballaran, T. (2004) New insight into the crystal structure of orthorhombic edingtonite: Evidence for a split Ba site. Mineralogical Magazine, 68, 167–175.

Gatta, G.D. and Wells, S.A. (2004) Rigid Unit Modes at high-pressure: an explorative study of a fibrous zeolite like framework with EDI topology. Physics and Chemistry of Minerals, 31, 465–474.

Gatta, G.D., Comodi, P., and Zanazzi, P.F. (2003) New insights on high-pressure behavior of microporous materials from X-ray single-crystal data. Microporous and Mesoporous Materials, 61, 105–115.

Gatta, G.D., Boffa Ballaran, T., Comodi, P., and Zanazzi, P.F. (2004a) Isothermal equation of state and compressional behavior of tetragonal edingtonite. American Mineralogist, 89, 633–639.

——— (2004b) Comparative compressibility and equation of state of orthorhombic and tetragonal edingtonite. Physics and Chemistry of Minerals, 31, 288–298.

Gatta, G.D., Comodi, P., Zanazzi, P.F., and Boffa Ballaran, T. (2005) Anomalous elastic behavior and high-pressure structural evolution of zeolite levyne.

American Mineralogist, 90, 645–692

Gianpaolo, C., Godano, R.F., Di Sabatino, B., and Barrese, E. (1997) The alteration of leucite-bearing rocks: A possible mechanism. European Journal of Mineralogy, 9, 1293–1310.

Gibbs, G.V., Rosso, K.M., Teter, D.M., Boisen, M.B. Jr., and Bukowinski, M.S.T. (1999) Model structures and properties of the electron density distribution for low quartz at pressure: A study of the SiO bond. Journal of Molecular Structure, 485–486, 13–25.

Gibbs, G.V., Boisen, M.B. Jr., Rosso, K.M., Teter, D.M., and Bukowinski, M.S.T. (2000) Model structures and electron density distribution for the silica polymorph coesite at pressure: An assessment of OO bonded interactions. Journal of Physical Chemistry B, 104, 10534–10542.

Goryainov, S.V., Fursenko, B.A., and Belitsky, I.A. (1996) Phase transitions in analcime and wairakite at low-high temperature and pressure. Physics and Chemistry of Minerals, 23, 297–308.

Gottardi, G. and Galli, E. (1985) Natural Zeolites, 409 p. Springer-Verlag, Berlin.

Hazen, R.M. and Finger, L.W. (1979) Polyhedral tilting: A common type of pure displacive phase transition and its relationship to analcime at high pressure. Phase Transitions, 1, 1–22.

Heinz, D.L. and Jeanloz, R. (1984) The equation of state of the gold calibration standard. Journal of Applied Physics, 55, 885–893.

Holl, C.M., Smyth, J.R., Laustsen, H.M.S., Jacobsen, S.D., and Downs, R.T. (2000) Compression of witherite to 8 GPa and the crystal structure of $BaCO_3$-II. Physics and Chemistry of Minerals, 27, 467–473.

Kapusta, J. and Wlodyka, R. (1997) The X-ray powder diffraction profile analysis of analcimes from the teschenitic sills of the Outer Carpathians, Poland. Neues Jahrbuch fuer Mineralogie, Monatshefte, 6, 241–255.

Kato, M. and Hattori, T. (1998) Ordered distribution of aluminum atoms in analcime. Physics and Chemistry of Minerals, 25, 556–565.

Kim, K.T. and Burley, B.J. (1971) Phase equilibria in the system $NaAlSi_3O_8$-$NaAlSiO_4$-H_2O with special emphasis on the stability of analcime. Canadian Journal of Earth Sciences, 8, 311–338, 549–558, 558–572.

——— (1980) A further study of analcime solid solutions in the system $NaAl$-Si_3O_8-$NaAlSiO_4$-H_2O with particular note of an analcime phase transformation. Mineralogical Magazine, 43, 1035–145.

King, H.E. and Finger, L.W. (1979) Diffracted beam crystal centering and its application to high-pressure crystallography. Journal of Applied Crystallography, 12, 374–378.

Lee, Y., Vogt, T., Hriljac, J.A., Parise, J.B., and Artioli, G. (2002a) Pressure-induced volume expansion of zeolites in the natrolite family. Journal of the American Chemical Society, 124, 5466–5475.

Lee, Y., Vogt, T., Hriljac, J.A., Parise, J.B., Hanson, J.C., and Kimk, S.J. (2002b) Non-framework cation migration and irreversible pressure-induced hydration in a zeolite. Nature, 420, 485–489.

Lee, Y., Hriljac, J.A., and Vogt, T. (2004a) Pressure-induced migration of zeolitic water in laumontite. Physics and Chemistry of Minerals, 31, 421–428.

Lee, Y., Hriljac, J.A., Studer, A., and Vogt, T. (2004b) Anisotropic compression of edingtonite and thomsonite to 6 GPa at room temperature. Physics and Chemistry of Minerals, 31, 22–27.

Line, C.M.B. (1995) The behaviour of water in analcime. Ph.D. Thesis, University of Cambridge, Cambridge, U.K.

Line, C.M.B., Putnis, A., Putnis, C., and Giampaolo, C. (1995) The dehydration kinetics and microtexture of analcime from two parageneses. American Mineralogist, 80, 268–279.

Line, C.M.B., Dove, M.T., Knight, K.S., and Winkler, B. (1996) The low-temperature behavior of analcime: I. High-resolution neutron powder diffraction. Mineralogical Magazine, 60, 499–507.

Liou, J.G. (1971) Analcime equilibria. Lithos, 4, 389–402.

Luhr, J.F. and Kyser, T.K. (1989) Primary igneous analcime: The Colima minettes. American Mineralogist, 74, 216–223.

Mao, H.K., Xu, J., and Bell, P.M. (1986) Calibration of the ruby pressure gauge to 800 kbar under quasi-hydrostatic conditions. Journal of Geophysical Research, 91, 4673–4676.

Martinez, I., Zhang, J., and Reeder, R.J. (1996) In-situ X-ray diffraction of aragonite and dolomite at high pressure and high temperature: Evidence for dolomite breakdown to aragonite and magnesite. American Mineralogist, 81, 611–624.

Mazzi, F. and Galli, E. (1978) Is each analcime different? American Mineralogist, 63, 448–460.

Merrill, L. and Bassett, W.A. (1972) Crystal structures of the high pressure phases of calcite. EOS, 53, 1121.

——— (1975) The crystal structure of $CaCO_3$ (II), a high pressure metastable phase of calcium carbonate. Acta Crystallographica, B31, 343–349.

Miletich, R., Allan, D.R., and Kush, W.F. (2000) High-pressure single-crystal techniques. In R.M. Hazen and R.T. Downs, Eds., High-Temperature and High-Pressure Crystal Chemistry. Reviews in Mineralogy and Geochemistry, 41, 445–519. Mineralogical Society of America and Geochemical Society, Washington, U.S.A.

Miroshnichenko, Y.M. and Goryainov, S.V. (2000) Raman study of high-pressure phase transitions in dehydrated analcime. Minaralogical Magazine, 64, 301–309.

Neuhoff, P.S., Stebbins, J.F., and Bird, D.K. (2003) Si-Al disorder and solid solutions in analcime, chabazite, and wairakite. American Mineralogist, 88, 410–423.

Oxford Diffraction (2003) Oxford Diffraction Ltd., Xcalibur CCD system, CrysAlis Software system, Version 1.170.

Pechar, F. (1988) The crystal structure of natural monoclinic analcime ($NaAlSi_2O_6$·H_2O). Zeitschrift fuer Kristallographie, 184, 63–69.

Pennington, W.T. (1999) DIAMOND-Visual Crystal Software Information System. Journal of Applied Crystallography, 32, 1028–1029.

Prelević, D., Foley, S.F., Cvetković, V., and Romer, R.L. (2004) The analcime problem and its impact on the geochemistry of ultrapotassic rocks from Serbia. Mineralogical Magazine, 68, 633–648.

Putnis, A., Giampaolo, G., and Graeme-Barber, A. (1993) High temperature X-ray diffraction and thermogravimetric analysis of the dehydration of analcime, $NaAlSi_2O_6$·H_2O. EUG VII, Strasbourg, France, Terra Abstracts, 5, 497.

Ralph, R.L. and Finger, L.W. (1982) A computer program for refinement of crystal orientation matrix and lattice constants from diffractometer data with lattice symmetry constraints. Journal of Applied Crystallography, 15, 537–539.

Redfern, S.A.T. (2000) Structural variations in carbonates. In R.M. Hazen and R.T. Downs, Eds., High-Temperature and High-Pressure Crystal Chemistry, 41, 289–308. Reviews in Mineralogy and Geochemistry, Mineralogical Society of America, Washington, U.S.A.

Redkin, A.F. and Hemley, J.J. (2000) Experimental Cs and Sr sorption on analcime in rock-buffered systems at 250-300 degrees C and Psat and the thermodynamic evaluation of mineral solubilities and phase relations. European Journal of Mineralogy, 12, 999–1014.

Ross, N.L. (2000) Framework Structures. In R.M. Hazen and R.T. Downs, Eds., High-Temperature and High-Pressure Crystal Chemistry. Reviews in Mineralogy and Geochemistry, 41, 257–287. Mineralogical Society of America and Geochemical Society, Washington, U.S.A.

Roux, J. and Hamilton, D. (1976) Primary igneous analcime; an experimental study. Journal of Petrology, 17, 244–257.

Sheldrick, G.M. (1997) SHELX-97. Programs for crystal structure determination and refinement. University of Göttingen, D.

Singh, A.K. and Kennedy, G.C. (1974) Compression of calcite to 40 kbar. Journal of Geophysical Research, 79, 2615–2622.

Smyth, J.R. and Ahrens, T.J. (1997) The crystal structure of calcite III. Geophysical Research Letters, 25, 1595–1598.

Takaishi, T. (1998) Ordered distribution of Al atoms in the framework of analcimes. Journal of the Chemical Society-Faraday Transactions, 94, 1507–1518.

Taylor, W.H. (1930) The structure of analcime ($NaAlSi_2O_6$·H_2O). Zeitschrift fuer Kristallographie, 74, 1–19.

Tribaudino, M., Benna, P., Bruno, E., and Hanfland, M. (1999) High pressure behavior of lead feldspar ($PbAl_2Si_2O_8$). Physics and Chemistry of Minerals, 26, 367–374.

Welch, M.D., Kleppe, A.K., and Jephcoat, A.P. (2004) Novel high-pressure behavior in chlorite: A synchrotron XRD study of clinochlore to 27 GPa. American Mineralogist, 89, 1337–1340.

Wilkinson, J.F.G. (1977) Analcime phenocrysts in a vitrophyric analcimite; primary or secondary? Contributions to Mineralogy and Petrology, 64, 1–10.

Wilson, A.J.C. and Prince, E. (Eds.) (1999) International Tables for X-ray Crystallography, Volume C: Mathematical, Physical and Chemical Tables (2nd edition). Kluwer Academic, Dordrecht, Netherlands.

Woolley, A.R. and Symes, R.F. (1976) The analcime-phyric phonolites (blairmorites) and associated analcime kenytes of the Lupata Gorge, Mocanbique. Lithos, 9, 9–15.

Yoder, H.S. Jr. and Weir, C.E. (1960) High-pressure form of analcime and free energy change with pressure of analcime reactions. American Journal of Science, 258A, 420–433.

Yokomori, Y. and Idaka, S. (1998) The crystal structure of analcime. Microporous and Mesoporous Materials, 21, 365–370.